

# We are IntechOpen, the world's leading publisher of Open Access books Built by scientists, for scientists

6,700

Open access books available

182,000

International authors and editors

195M

Downloads

Our authors are among the

154

Countries delivered to

TOP 1%

most cited scientists

12.2%

Contributors from top 500 universities



WEB OF SCIENCE™

Selection of our books indexed in the Book Citation Index  
in Web of Science™ Core Collection (BKCI)

Interested in publishing with us?  
Contact [book.department@intechopen.com](mailto:book.department@intechopen.com)

Numbers displayed above are based on latest data collected.  
For more information visit [www.intechopen.com](http://www.intechopen.com)



## Chapter

# Discussion

*Yasuto Itoh, Akio Hara and Taiki Sawada*

## Abstract

The subsurface structure and sedimentary facies in the Beppu Bay basin were studied using 2D seismic and 3D high-resolution seismic (3D-HRS) surveys. A series of high-angle faults extend near the southern bay coast and are interpreted as active traces of the laterally moving Median Tectonic Line (MTL). A releasing bend of the MTL forms a pull-apart sag around the bay bottom accompanied by numerous normal fractures, whereas a compressional bulge is emerging on the southern side of the bay, suggesting complicated and transient stress states in the late Quaternary strata. Based on the general development history of the Hohi Volcanic Zone (HVZ), the lower, middle, and upper seismic horizons are assigned to 5–6 Ma (initial stage of the HVZ), 0.7 Ma, and 0.3 Ma, respectively. We identified three auxiliary reflectors within the upper part of the sediment pile and correlated them with oxygen isotope stages 15–11. These stratigraphic constraints are used to discuss paleoenvironments in the latest Pleistocene by means of an amplitude root mean square attribute analysis of the 3D-HRS data, which successfully delineated a buried river channel that was active during the last glacial period.

**Keywords:** Beppu Bay, Median Tectonic Line, seismic interpretation, seismic attribute, paleoenvironment

## 1. Introduction

As documented in Chapter 3, the latest technology of 3D high-resolution seismic (3D-HRS) surveying has successfully delineated fine structural features within the analyzed volume around the mouth of Beppu Bay (**Figure 1**) adjacent to the previous 2D seismic lines. In this chapter, we describe the deep fault architecture and stress–strain state around the bay in a wider scope using the conventional 2D data [1] and then discuss the possible transition of the pull-apart depocenter based on available age constraints of notable reflectors in the seismic profiles. Finally, the potential value of attribute analyses of the 3D-HRS dataset is presented from the viewpoint of paleoenvironmental interpretation.

## 2. Complicated stress distribution around Beppu Bay

**Figure 2** shows a bird’s-eye view of the subsurface structure of Beppu Bay [1, 2]. As depicted in profiles E and H, a series of high-angle faults having a “flower-like” appearance extend near the southern margin of the bay. Previous studies [2–4] interpreted that this fault zone is an active trace of the dextral Median Tectonic Line (MTL). Around the

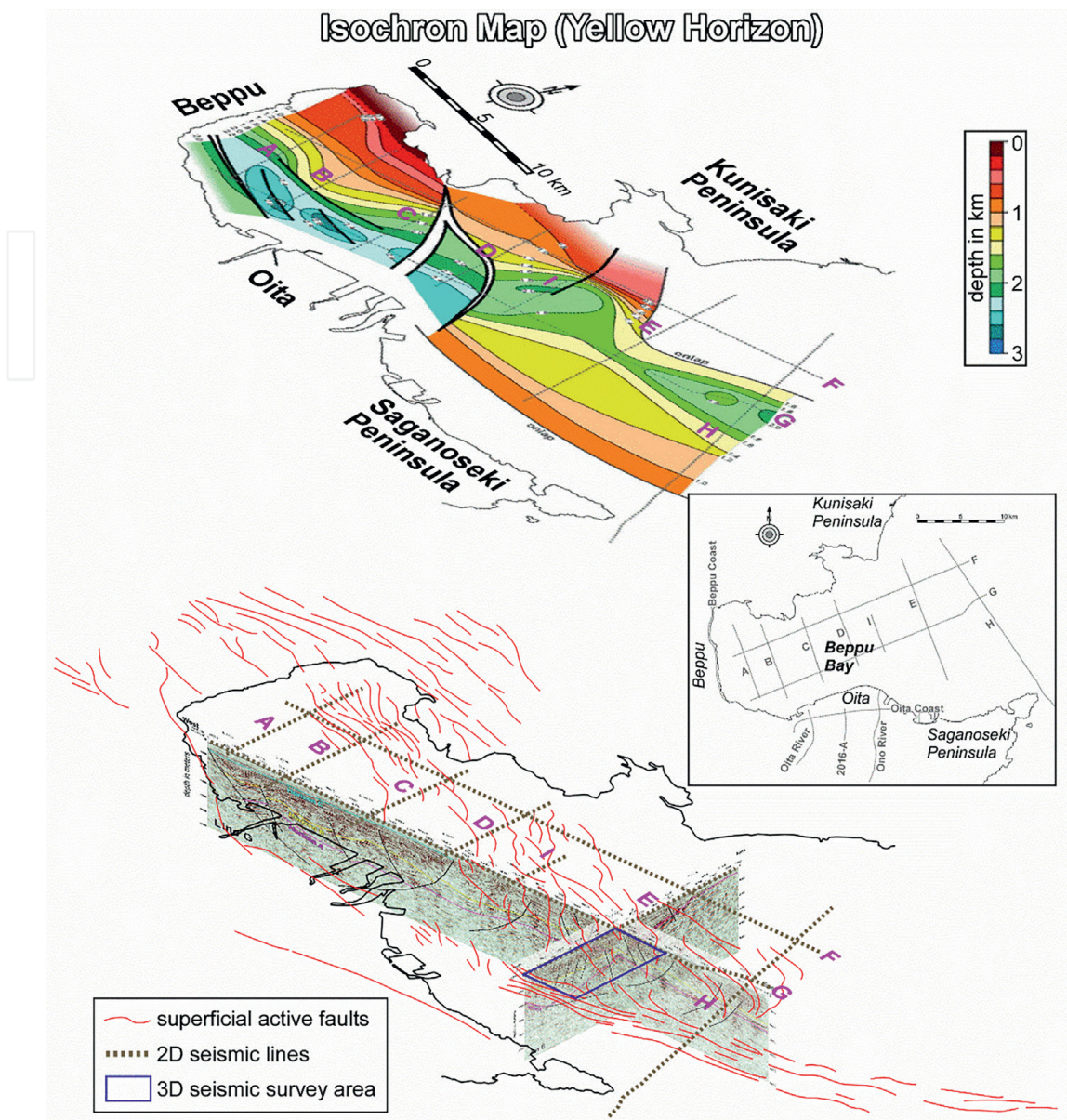


**Figure 1.** Seismic survey index maps of the study area. The isochron map of the Pleistocene seismic horizon (upper) is after [1].

bay bottom (westernmost part), a releasing bend of the MTL has formed a pull-apart sag, the outline of which can be traced along numerous normal fractures in the shallows (red lines in **Figure 1**). Although such extensional features are suggestive of a prevalent tensile stress field [5]; Itoh and Inaba [2] argued that a compressional bulge is growing under the southern bay coast from the structural interpretation of recent obvious inversion on a seismic section (**Figure 2b**). Thus, Beppu Bay is characterized by a complicated and transient stress state during the late Quaternary. Temporal constraints on the architectural buildup of the study area are discussed in the next section.

### 3. Age assignment of seismic horizons

The Quaternary system exposed around the bay is dominantly composed of volcanoclastic material derived from a number of active volcanoes. Their varied lithofacies



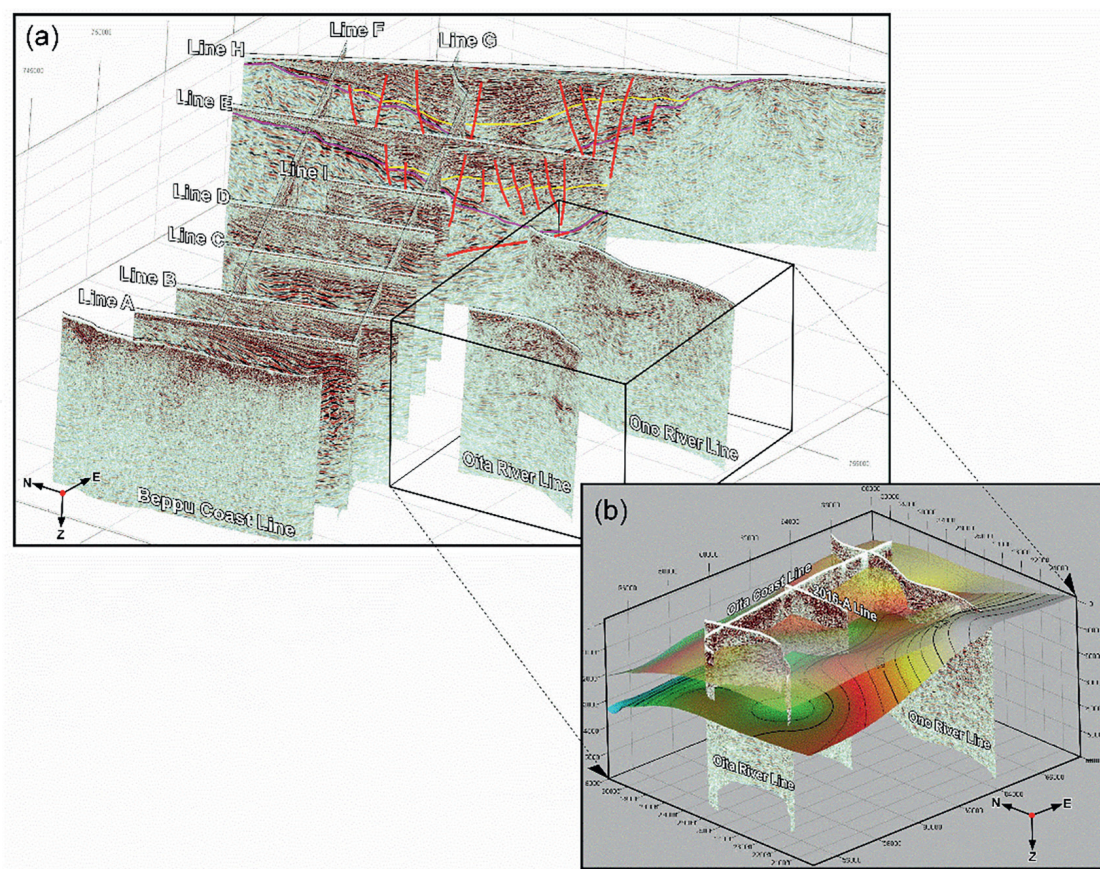


**Figure 2.**  
Bird's-eye views of the 2D seismic data (modified from [1]) around Beppu Bay.

and absence of index fossils hinder precise stratigraphic correlation. Moreover, the ages of significant seismic horizons have not been established for the sediments filling the Beppu Bay basin due to the lack of borehole data. To overcome such difficulties, we assign numerical ages to conspicuous horizons based on major geologic events recorded in terrigenous sediments. **Figure 3** presents our stratigraphic model. Based on the general development history of the Hoho Volcanic Zone (HVZ) tectonic graben [4], the bottom of the basin fill (Horizon A) is assumed to be 5–6 Ma. Another ubiquitous horizon (B) in the middle of the sediment pile is correlated with an unconformity at the basal part of the Oita Group (ca. 0.7 Ma [6]). The uppermost Horizon C, traceable within the western half of the bay, coincides with a drastic change in seismic facies and is interpreted as the cessation of clastic supply from the Hiji volcano on the northern coast (ca. 0.3 Ma [7]). Major seismic datum levels are thus assigned to volcano-tectonic events.

Other semicontinuous reflectors are probably related to paleoenvironmental changes. Beppu Bay is an estuary up to of 70 m deep, and it has inevitably experienced marine/nonmarine transition according to eustatic changes in sea level. Previous stratigraphic studies in similar environments [8, 9] showed that traceable seismic reflectors are linked with basal horizons of marine clays, which are clearly recognized by sharp lithologic changes, and have straightforward correspondence to the oxygen isotope record during rapid marine transgression. Based on these chronological constraints, the evolution and migration of pull-apart basins in the bay area is reconstructed in the next section.



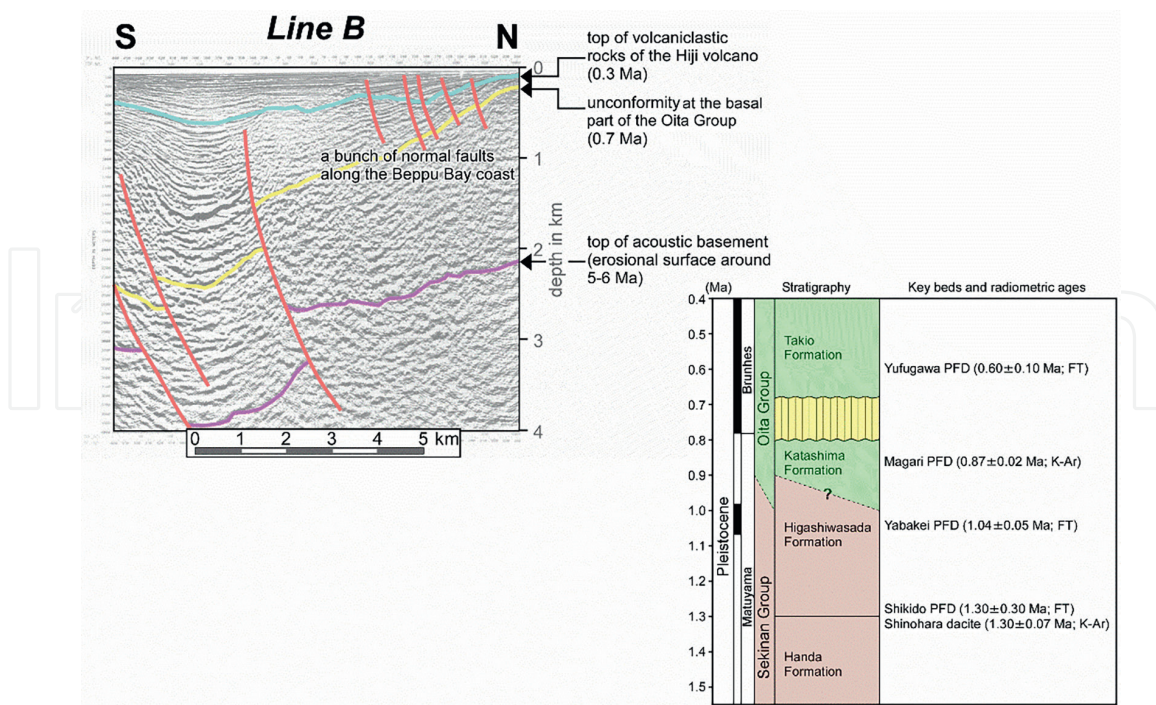


**Figure 3.** Chronological framework of 2D seismic horizons and stratigraphic summary of the Quaternary system exposed around Beppu Bay. See the text for data sources.

#### 4. Depocenter migration within Beppu Bay

**Figure 4** presents a record of a 2D seismic line running from the bottom (west) to the mouth (east) of the bay. The major horizons A, B, and C described above are traced on the profile and delineate remarkable fault-bounded depressions. The two depocenters accompanied by extensional features are clearly seen. They are aligned along the MTL active fault system (**Figure 2**) and interpreted as a series of pull-apart basins. It is noteworthy that the displacement growth on the faults bounding the western depocenter is indicative of ongoing subsidence, whereas the eastern one seems to have been dormant in recent periods. This phenomenon is probably related to depocenter migration provoked by terminal propagation of the MTL, as is often the case with large transcurrent faults (e.g., [11, 12]).

Based on their numerical ages, Horizons B and C are assigned to global oxygen isotope stages 17 and 9, respectively (after [10]). Between these controlling datum levels are three auxiliary reflectors (see **Figure 4**). As explained in the previous section, they originate from eustatic marine transgression and are correlated with marine isotope stages (MISs) 15–11 (odd numbers) in ascending order, considering the stratigraphic framework. Thus, an evolutionary overview of Beppu Bay, described by Itoh and Inaba [2], is obtained from the 2D seismic interpretation.

#### 5. Insight into paleoenvironments

##### 5.1 3D seismic interpretation

The 3D-HRS survey data were acquired by Kyoto University and JGI, Inc., within Beppu Bay. The survey area location, ranging 3 km by 6 km in the bay and located

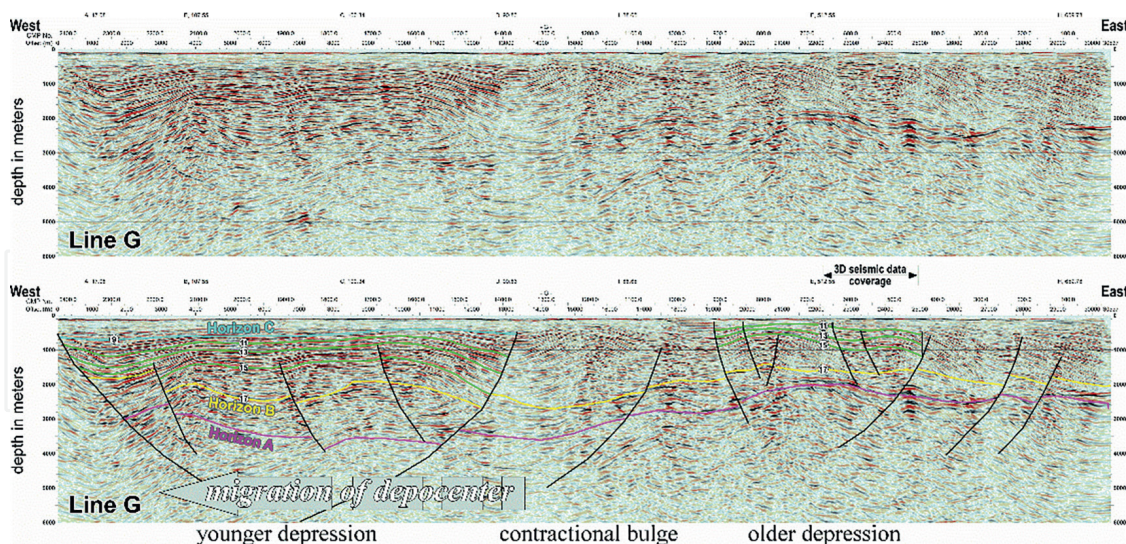


**Figure 4.** E-W seismic profile (G; see **Figures 1 and 2** for location) in Beppu Bay. Raw section (top) and interpreted section (bottom) are shown after depth conversion. See **Figure 3** for numerical ages of the controlling horizons. Annotation numbers on the major and minor (green) horizons are oxygen isotope stages after Lisiecki and Raymo [10].

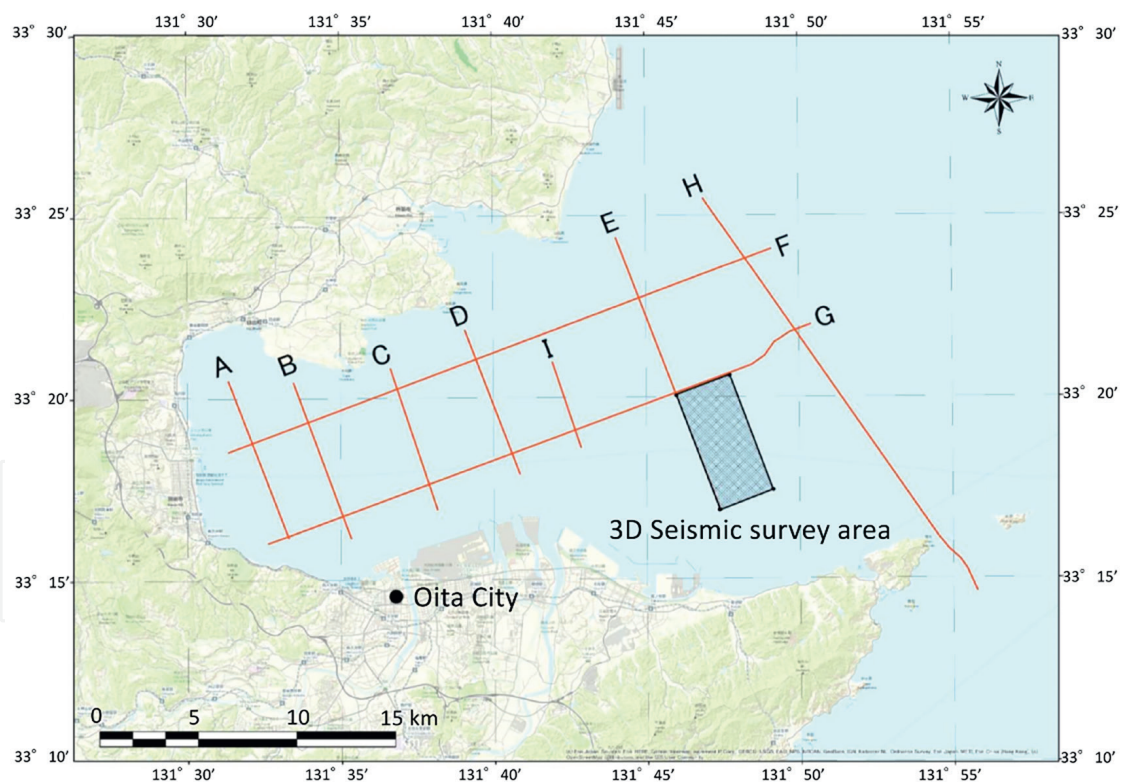


**Figure 5.** Location map of the 3D seismic survey area.

15 km northeast offshore of Oita City (Oita Prefecture), is shown in **Figure 5**. The northern and western edges of the survey area are in contact with the existing 2D seismic survey lines G and E, respectively.

Geological interpretation work was carried out by combining the geological structure interpretation obtained by tracing the reflecting surface and the attribute



| Horizon     | Age         | Remarks   |
|-------------|-------------|---|
| Light Blue  | Recent      | Sea floor   |
| Blue        | Holocene    | Base of Alluvial                                      |
| Orange      | Pleistocene | Base of High amplitude unit                           |
| Yellow      |             | Reflective surface with good continuity. Age unknown. |
| Pink        |             |   |
| Green       |             |   |
| Light Green |             | MIS-11 (Estimated)                                    |
| Magenta     |             | MIS-13 (Estimated)                                    |

**Table 1.**

List of interpreted horizons used for geological interpretation.

analysis obtained by applying the amplitude root mean square (RMS). For the geological interpretation, we selected eight reflective surfaces that can be traced continuously within the survey area. **Table 1** shows the names and characteristics of each horizon. The lowest magenta horizon is a reflective surface that can be compared with the MIS-13 horizon (ca. 0.49 Ma) estimated from the 2D cross section shown in **Figure 4**. Also, the light green horizon can be compared to MIS-11 (ca. 0.41 Ma). The green, pink, yellow, and orange horizons are all presumed to be Pleistocene, but their ages are unknown. The blue horizon is an unconformity surface and is presumed to be the base of the Holocene deposits because modern seafloor sediments have accumulated above it. The interval between the orange and blue horizons can be characterized by a predominance of high-amplitude reflective surfaces.

**Figures 6–9** show examples of geological cross sections. **Figure 6** is a cross section of Inline 251 that cuts through the center of the survey area from north to south, with north on the right. The depth to the seafloor is about 25 m at the southern end of the survey line and gradually increases toward the north, reaching a depth of about 40 m at the northern end of the survey line. A local depression is present on the seafloor near the intersection with Crossline 1100. At this position, the normal fault can be interpreted as being near the seafloor, and the hanging wall (north side of the fault plane) has subsided relative to the south side of the fault. Seismic facies between the seafloor (light blue horizon) and the alluvium base (blue horizon) can be characterized by a predominance of low-amplitude reflectors with good lateral continuity. The alluvium becomes thinner and almost completely vanishes at the southern end of the survey line but reaches a maximum at the northern end of the survey line at about 50 m. In addition, the layer thickness increases locally on the north side of the fault at Crossline 1100. The alluvium base is an unconformity surface, and the underlying reflective surface is cut by the alluvium base. Underneath the alluvium base strata, the geology is dominated by discontinuous, strong-amplitude reflective surfaces. This geologic unit is composed of multiple strongly reflective surfaces, and the base of this unit is traced as a high-amplitude base horizon (orange horizon).

The thickness of the geological body is about 30 m at the north end of the survey line, but it is denuded by the alluvium base near Crossline 700 and disappears. The age of this geological unit is estimated to be Pleistocene because it is directly denuded by the alluvium base. The strongly reflective surfaces below the orange horizon are identified and tracked as yellow, pink, green, light green, and magenta from the top.

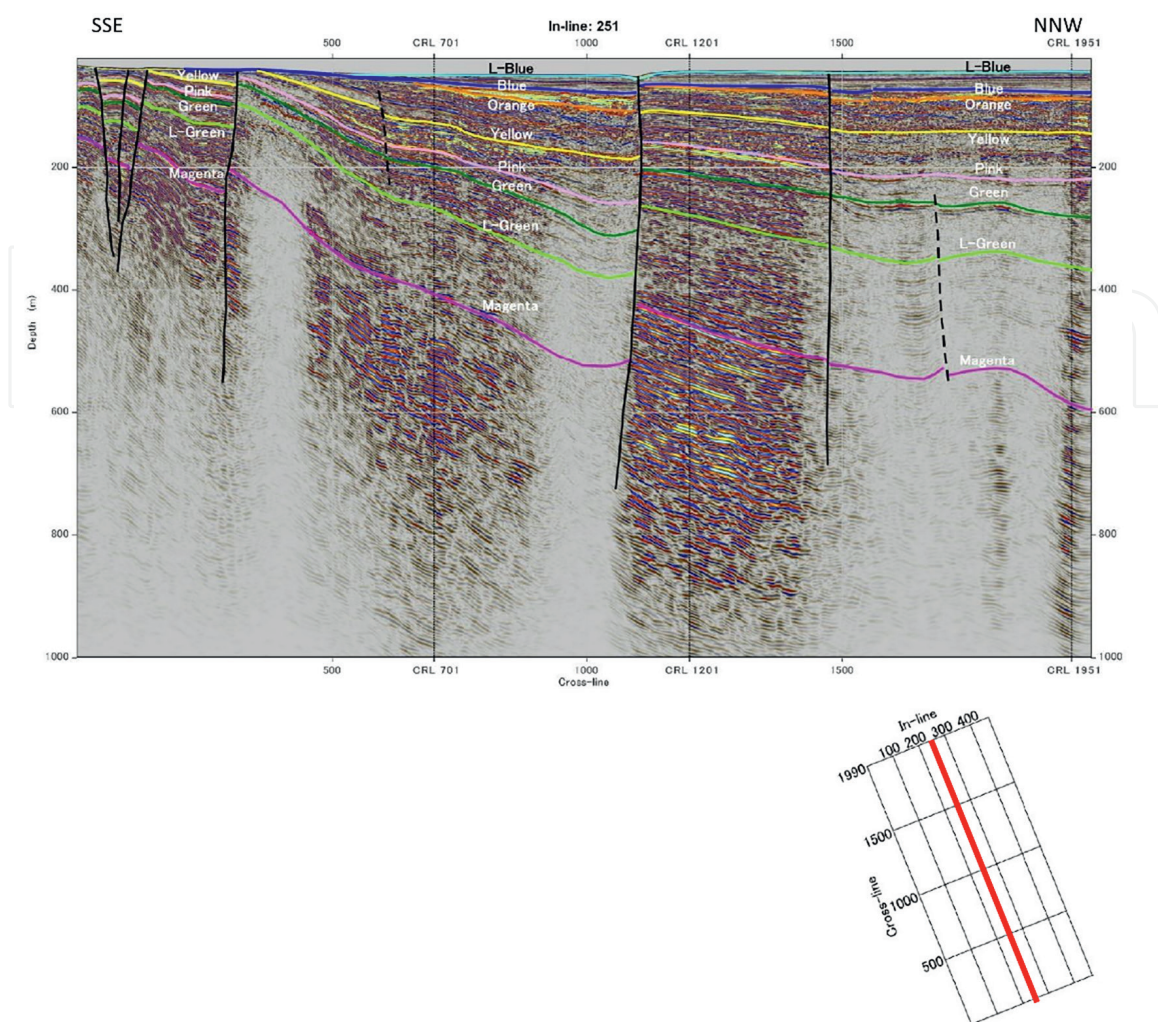


**Figure 6.** Geological interpretation section of inline 251. Thick black lines are faults. Light green and magenta horizons are assigned to the MIS-11 and MIS-13 horizons [10], respectively.

It is difficult to determine the geological age because no boreholes have been drilled into the research area. Between the orange and yellow horizons, reflective surfaces with relatively low amplitude and poor continuity predominate. The layer thickness of this section is about 60 m at the north end of the survey line, but it tends to become thinner toward the south. Between the yellow and pink horizons, a reflective surface with a strong amplitude but poor continuity dominates. The layer thickness is about 70 m at the north end of the survey line, and it decreases toward the south to about 40 m at the south end of the survey line. The green horizon can be characterized by a continuous strong-amplitude reflective surface. The reflective surfaces between the pink horizon and the green horizon are dominated by relatively low-amplitude reflective surfaces with poor continuity. Reflective surfaces in the section from the green horizon to the magenta horizon can be characterized by weaker amplitudes and more prominent reflective surfaces with good continuity compared to that of the upper sections. The layer thickness between the green horizon and the light green horizon is about 70 m at the north end of the survey line and about 20 m at the south end of the survey line. The layer thickness of the light green and magenta horizons is about 200 m at the north end of the survey line and about 50 m at the south end of the survey line.



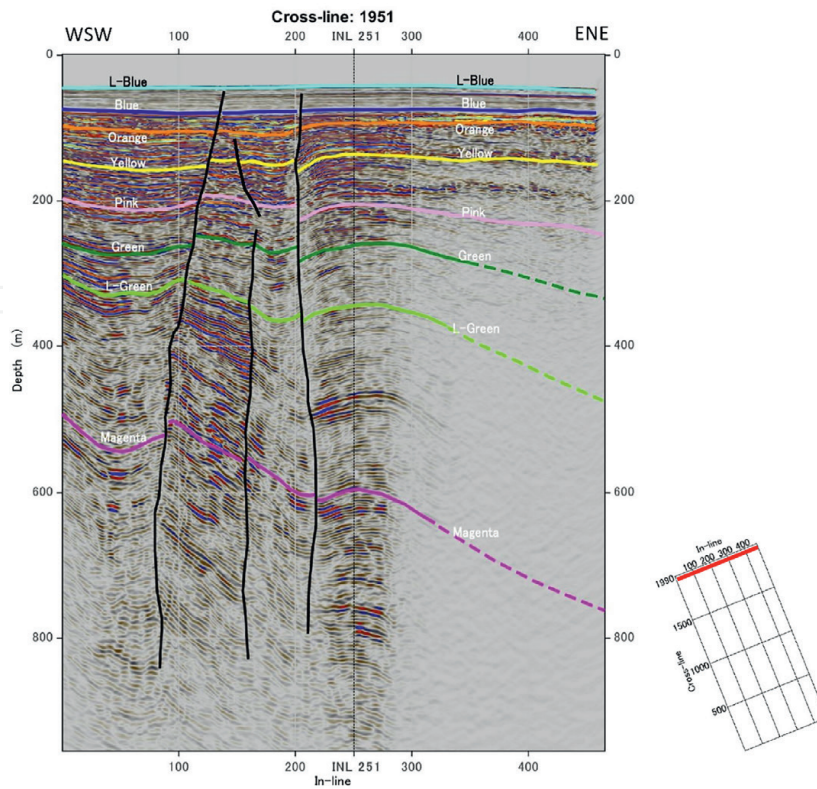


**Figure 7.** Geological interpretation section of crossline 1951. Thick black lines are faults. Light green and magenta horizons are assigned to the MIS-11 and MIS-13 horizons [10], respectively.

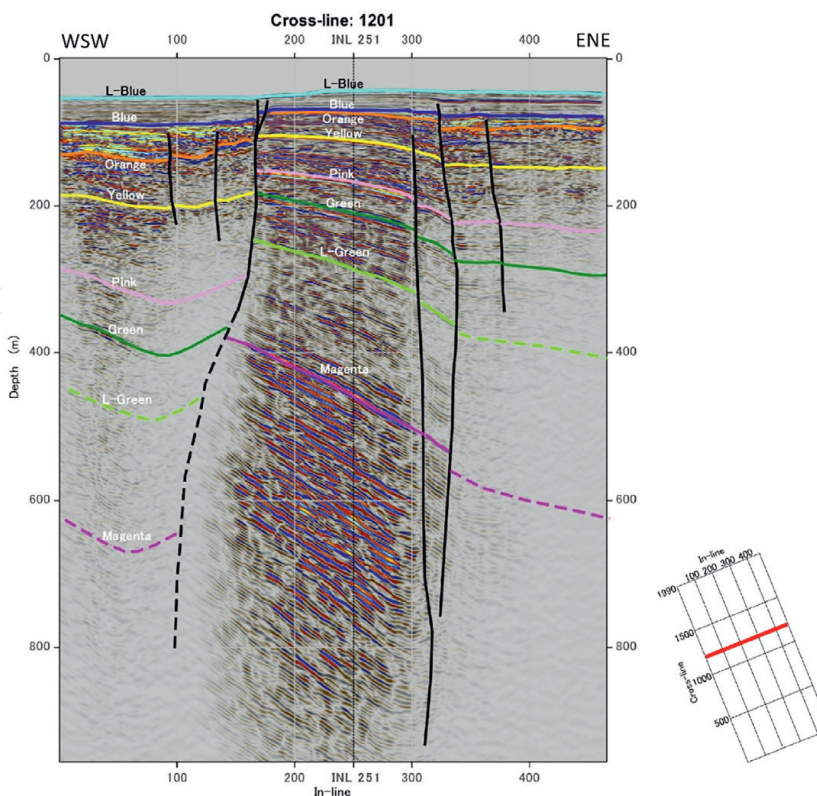


**Figure 8.** Geological interpretation section of crossline 1201. Thick black lines are faults. Light green and magenta horizons are assigned to the MIS-11 and MIS-13 horizons [10], respectively.

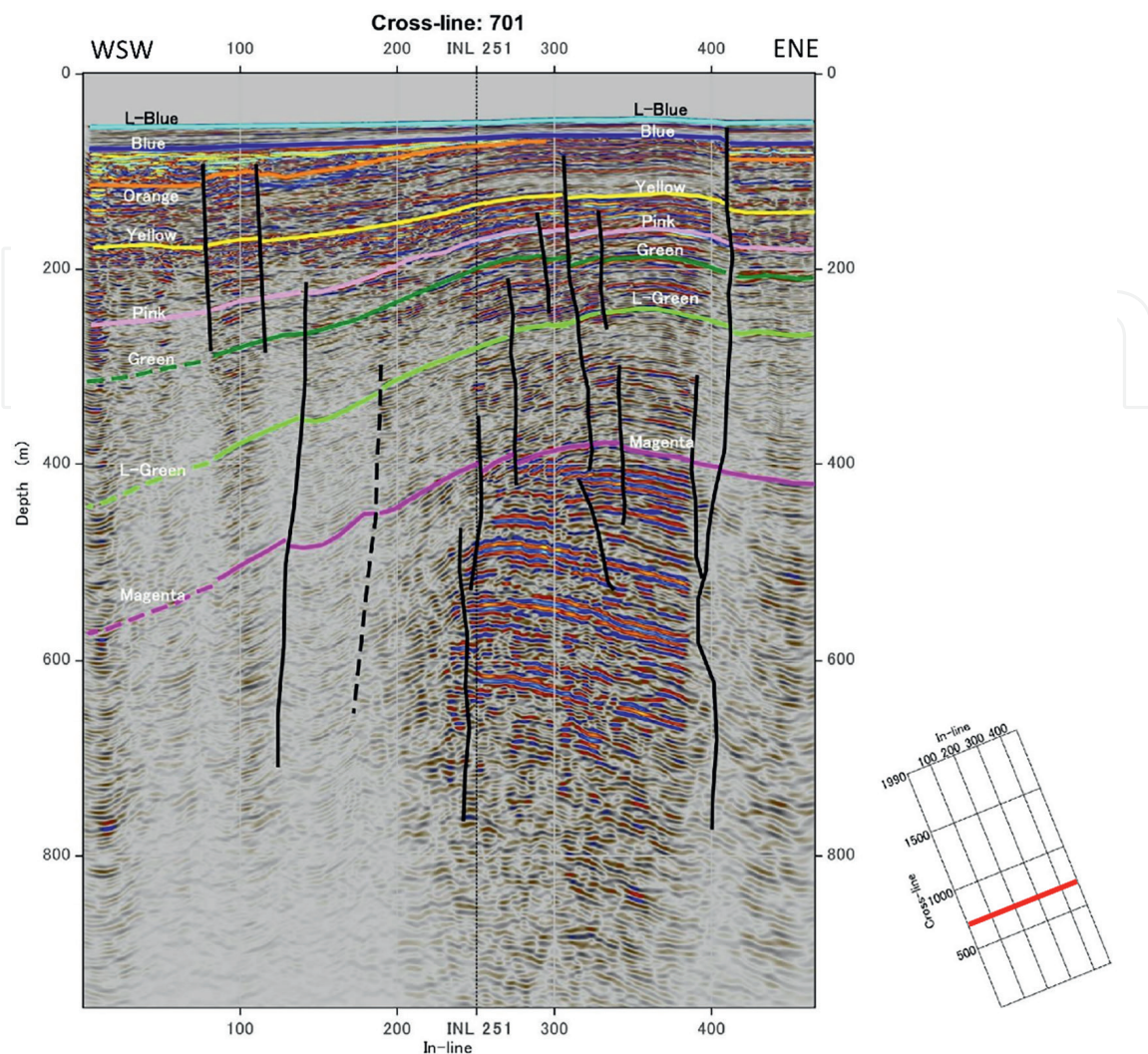


**Figure 9.** Geological interpretation section of crossline 701. Thick black lines are faults. Light green and magenta horizons are assigned to the MIS-11 and MIS-13 horizons [10], respectively.

**Figure 7** shows the geological interpretation of Crossline 1951. This cross section is located at the northern end of the 3D seismic survey and is close to the existing 2D survey line G [13], so it can be compared. In this chapter, we compare the geological ages of the reflection surfaces on line G with the high sea level period from MIS-17 to MIS-9 (see **Figure 4**). Regarding the 3D data acquisition range, MIS-13 and MIS-11, which are distributed at a depth of less than 1000 m, are compared with the magenta horizon and light green horizon, respectively.

The thickness distribution of strata in Crossline 1951 tends to increase toward the northeast side (right side). Three high-dip faults can be identified near the center of the cross section. A synclinal structure is formed on the reflecting surface that is in contact with the westernmost fault. In addition, an anticline structure can be identified on the northeast side of the easternmost fault. The reflecting surface in the section between these two faults (generally the section between Inlines 100 and 200) dips to the east, and the dip tends to increase with depth. In addition, at the eastern edge of this section (e.g., Inline 200, depth 600 m), a local synclinal structure can be discerned near the contact with the fault. The azimuth and dip of the fault plane are not constant, and a locally bulging shape can be seen (e.g., Inline 100, depth 400 m).



**Figure 8** shows the geological interpretation of Crossline 1201. The geological block in the center of the cross section, the section from Inlines 170 to 320, is bounded by faults and slopes eastward. It can be seen that the dip angle tends to increase as the depth increases. The geological unit from the western edge of the cross section to Inline 170 has subsided greatly along the fault plane, and the alluvium is thicker than the central geological block, reaching approximately 40 m. It is accompanied by multiple small-scale normal faults, and a flower-like structure can be seen. In addition, for the geological unit east of Inline 320, we can interpret the geological “flower” structure as comprising multiple normal faults. At Crossline 1201, both sides of the central geological block subside due to normal faults.

**Figure 9** shows the result of interpretation of Crossline 701. At Crossline 701, the west-dipping geological structure is dominant. Many small-scale, high-dip faults are formed near Inline 300, and individual blocks bounded by faults tilt to the west, forming a sawtooth-like structure. This situation has been interpreted in the pink and green horizons. The fault located at Inline 400 is a normal fault, and the adjacent eastern geological unit is subsiding. In the section from Crosslines 250 to 400, the dip of the reflecting surface to the east with the anticline axis near Inline 270 below the magenta horizon is dominant, and above that, the position of the anticline axis is eastward. Around the yellow horizon, the west-dipping structure around Inline 370 becomes dominant.

Geological interpretation work was conducted using 3D high-resolution earthquake exploration data. **Figure 10** shows the depth structural diagram of the seabed (light blue), the offshore layer base (blue), and the update (yellow and green). The inset shown at the upper left is the depth structure of the seabed surface. The water depth is about 30 m at the southern end near the coast, and the depth increases farther offshore, becoming about 40 m around Crossline 400. There is a distinctive trend in the depth distribution on the north side of Crossline 400. The most distinctive seabed terrain is cliff-like terrain that is linearly distributed on the line connecting Inline 1, Crossline 1501 and Inline 451, Crossline 801. The southwest side of the cliff is sinking, forming the deepest water area that exceeds a depth of 50 m. Another topographical characteristic is a ridge-like terrain extending northwest along Inline 351. The water is deeper toward both sides (northwest and southeast) on the ridge.

One of the characteristics of the depth distribution in each layer below the sea floor is two linear geological structures caused by the fault. One is on a line connecting Inline 1, Crossline 1401 and Inline 451, Crossline 901, and the other starts around Inline 200, Crossline 1990; passing Inline 351, Crossline 801; and reaching near Inline 451, Crossline 601. Here, the former is called Fault 1, and the latter is called Fault 2. For Fault 1, the block southwest of the fault is subsiding. Regarding Fault 2, the northeast side of the fault is subsiding. Judging from the depth contour of the geological block sandwiched between Faults 1 and 2, an anticline extending along the fault is formed at the southwestern end of the block, and it seems to dip toward the northeast. The geological block on the southwest side of Fault 1 is sloping toward the northwest and is deepest near the fault. It is possible that this geological block forms a half-graben-like structure. In contrast, the block on the northeast side of the Fault 2 is tilted in the northeast direction.

## 5.2 Attributes of 3D seismic data

The RMS of the amplitude was applied to the 3D seismic survey data acquired in Beppu Bay to perform a survey attribute analysis. The RMS attribute was calculated as a high-amplitude zone in the section of the window containing the trace if the

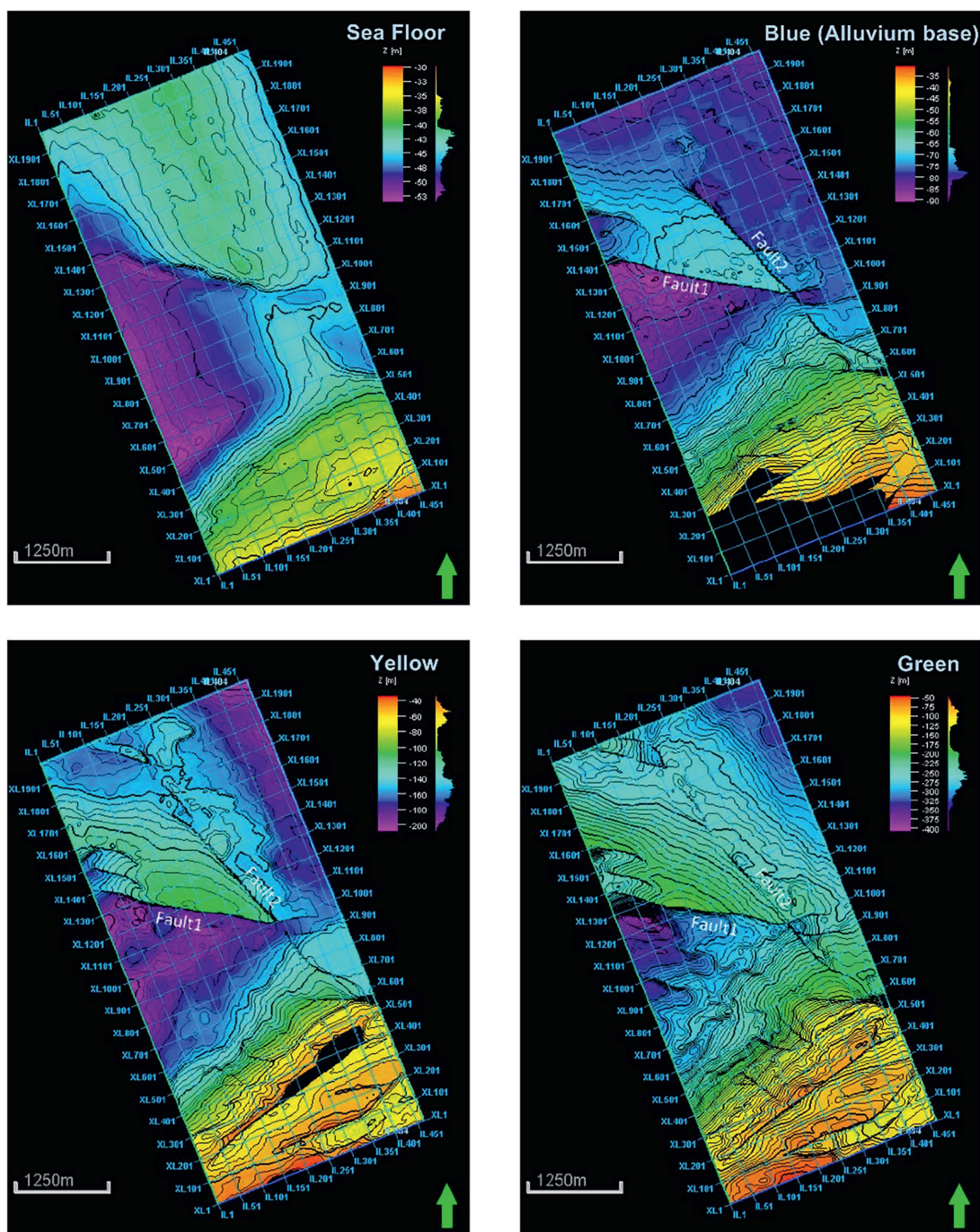


**Figure 10.**  
 Geological structure map of the sea floor, alluvium base, and Pleistocene deposits (yellow horizon and green horizon).

window section contains a trace sample with a large amplitude. The value was calculated for one trace of the seismic data, while that trace was moved over another trace by setting an arbitrary interval. The RMS amplitude attribute was calculated for the RMS of the amplitude value included in the seismic survey data. As an example of the reflection surface formed by a high amplitude, it was possible to identify a geological layer boundary where the difference between the impedance of the geological layer (product of the acoustic wave velocity and the density) increases. In the field of petroleum exploration, the RMS magnitude attribute is applied, and many cases of sandstone reservoirs with large impedances are used for the examination of their



distributed areas (e.g., [14, 15]). In this study, Landmark Solution's SeisSpace®/ ProMAX® was used for attribute analysis. The window size for calculating the RMS attribute was 11 samples (5 m).

**Figure 11** shows the analysis results for amplitude RMS. The top-left image is a slice section of the amplitude RMS at a depth of 87 m, and the top-right image is the amplitude RMS at a depth of 76 m. At 87 m, the pattern of a meandering river is continuously observed from Inline 1, Crossline 600 to the northeast direction, in the green to red area showing high-amplitude RMS, and the blue area showing low-amplitude RMS can be tracked. The 87-m level is located in the depth interval from the orange horizon to the alluvium base (blue horizon) where the high-amplitude reflector is dominant. Therefore, it is estimated that the amplitude RMS also increases in this section. In contrast, the river sediment RMS has a smaller amplitude than that of the surrounding strata, making it possible to extract the pattern of the river channel. The top-right image in the figure is the amplitude RMS at a depth of 76 m. In this slice section, we were able to capture an amplitude RMS pattern indicative of the meandering river within an area where such a pattern

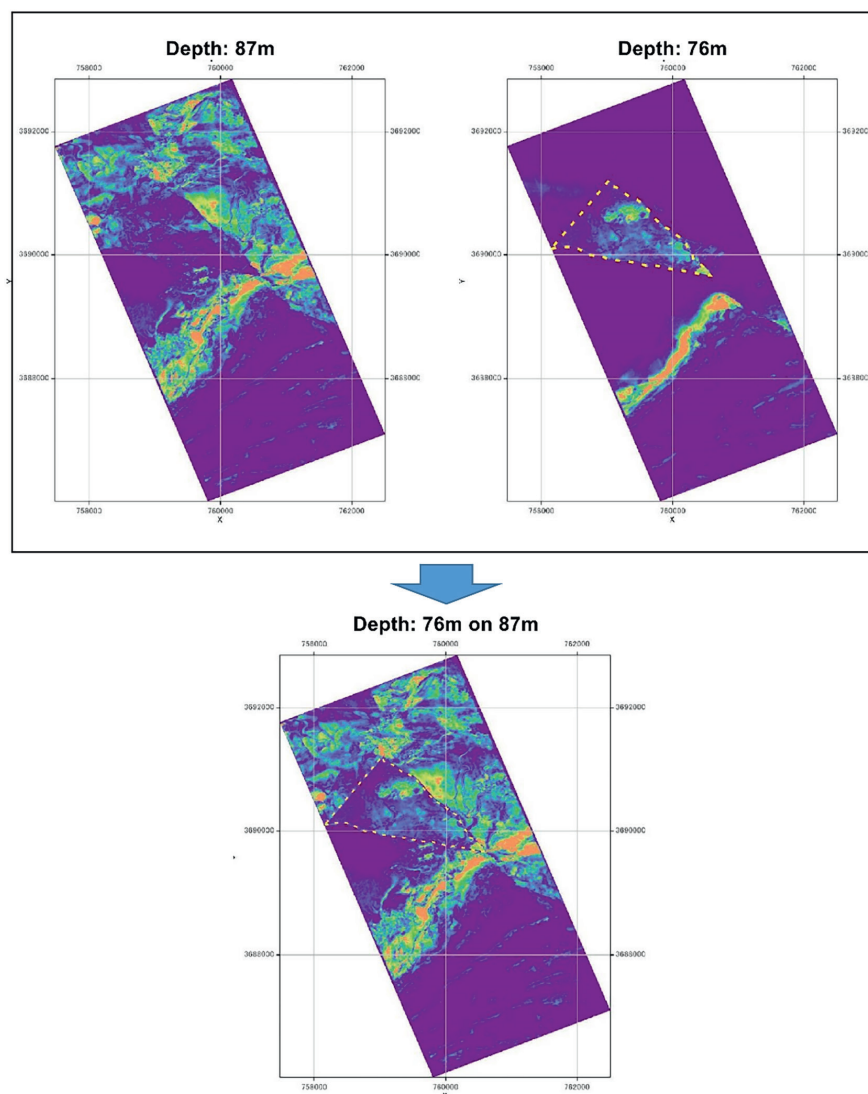


**Figure 11.** Mosaic map of the old channel. Top left: Depth at 87 m. top right: Depth at 76 m. Bottom inset shows a combined map.

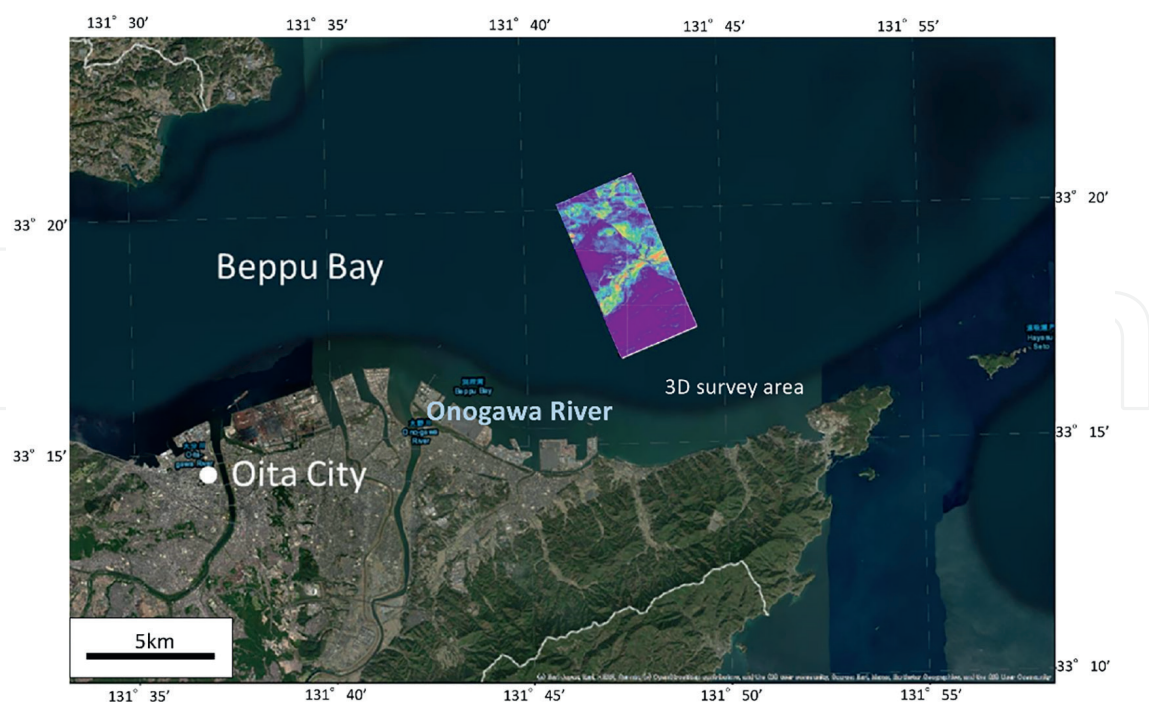


**Figure 12.**

*Comparison between the position of the old channel extracted from the amplitude RMS analysis result and the current river position.*

was missing in the slice section at 87 m. In the lower panel of **Figure 11**, which is a mosaic of amplitude RMS slices at both depths, the continuous meandering river pattern can be discerned.

**Figure 12** shows the location of the channel extracted from the amplitude RMS attribute analysis in a satellite landscape. The river channel extracted from the amplitude RMS attribute flows from the southwest to the northeast near the center of the 3D seismic survey area. Because the river is divided into multiple channels, it is estimated that the river flowed through a floodplain and its channel changed several times. Based on this river channel distribution and the spread of the floodplain, it is highly likely that the channel will continue to the vicinity of the present-day Onogawa River if it is traced upstream. The Onogawa River is a river that flows northeastward through the eastern half of the Oita Plain. The 3D survey area is located on the extension of the current Onogawa River. There are no large rivers in the eastern Oita Plain. Judging from the extent of the present-day delta for the Oita Plain, the Onogawa River is considered to be the most likely river to have reached the 3D survey area during low sea level periods.

### 5.3 Geological structure that regulates the position of the old channel

**Figure 13** shows a distribution diagram of the old channel in the slice of the geological interpretation section of Crossline 701 and the amplitude RMS with a depth of 87 m. The two yellow arrows shown at the western end of the geological interpretation section indicate the position where the old channel intersects this cross section. In this cross-sectional view, local undulations associated with faults are formed near the channel. The channel is located in a local concave area (near Inline 115), which is locally high (near Inline 90), and a high-rising edge. This suggests that the old channel of this era may have been controlled by the local uplift associated with the fault.



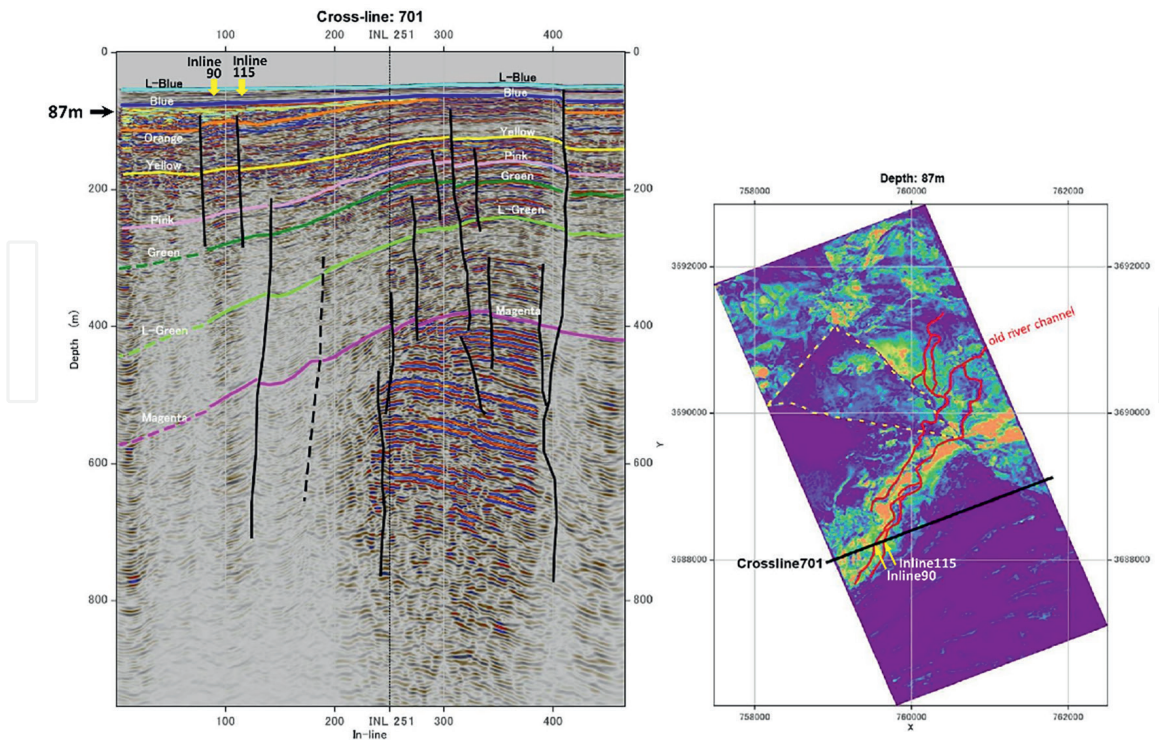


**Figure 13.**  
Characteristics of the geological structure where the channel was formed, as seen in the seismic section.

**Figure 14** shows the old channel flow path extracted from the results of the attribute analysis on the depth structure map of the orange horizon, where the channel is extracted. The channel is displayed as a red solid line. In this figure, the old river channel tends to have been formed in concave terrain and is consistent with the location of the old river path interpreted from the seismic section. An unconformity exists between the strata where the old channel was extracted and the alluvium, so it is difficult to identify the age of the sediments containing the old channel. However, considering that the depth difference from the basement of the alluvium is about 10 m, it is possible that the channel was formed during the late Pleistocene (near Holocene).

The bottom left of **Figure 14** shows the old river channel (solid red line) extracted as a result of attribute analysis superimposed on the depth map of the base of Holocene deposits (alluvium). In this figure, in the section from In-line 1 to In-line 350, the azimuth of the base of the alluvium is sloping northwest, while the old channel is diagonal. For this reason, it is difficult to assume that the river flowed in the northeast direction here. The bottom-right inset in **Figure 14** shows the old river channel superimposed on the current seafloor topography. In the section from In-line 1 to In-line 350, the channel is located on the slope of an up-dip. This suggests that the Onogawa River cannot flow northeastward through this section. Considering this series of trends, it is possible that the subsidence of the geological block located in the southwest direction progressed in this vicinity after the age when the old channel was formed. In the geological interpretation section shown in **Figure 13**, the anticline axis of the magenta horizon is located near In-line 300, but above it, the position seems to be gradually shifting to the east. This tendency seems to be consistent with the estimation that the Onogawa River had difficulty flowing northeastward during the geological age above the orange horizon.

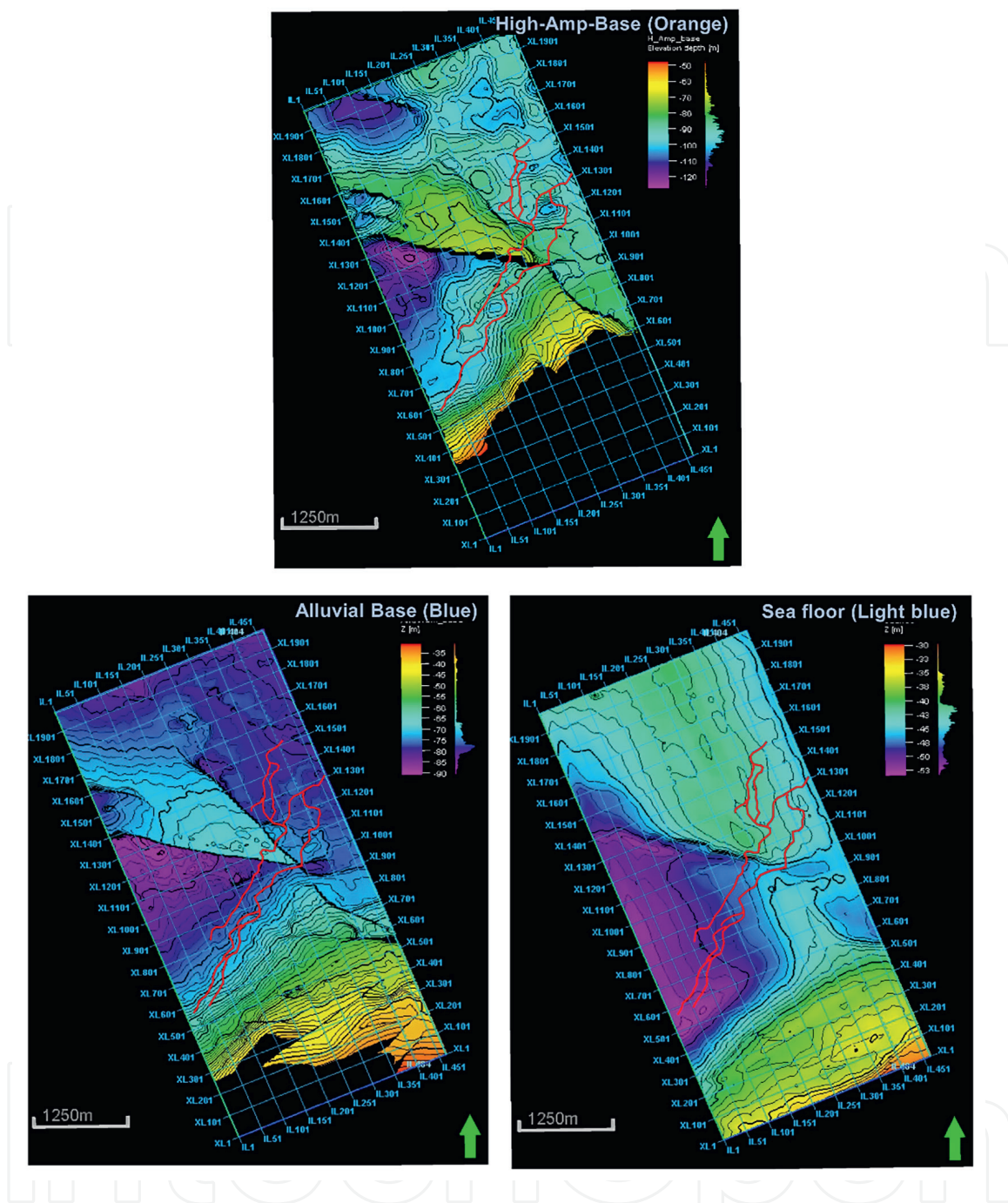


**Figure 14.** Comparison between the terrain of the era when the old river channel was formed and the terrain of the subsequent geologic periods.

## 6. Conclusion

In this chapter, we considered the growth process of the pull-apart basins in Beppu Bay, which are thought to have formed with right-lateral movements on the MTL based on the existing 2D seismic survey data. In the paleoenvironmental discussion, the latest 3D high-precision seismic survey data elucidated the following points.

1. As a result of interpreting the high-resolution 3D seismic profile obtained in the southern region of Beppu Bay, the stratigraphic horizon of an unconformable



surface was assigned to the Holocene base, and lower stratigraphic horizons were extracted for comparison with MIS-13 and MIS-11.

2. Two faults (Faults 1 and 2) were detected near the center of the northern half of the 3D seismic survey data. These faults intersect at an acute angle. The “inverted triangular” geologic block between the faults is tilting to the northeast. In addition, a local anticline structure is formed along Fault 1 at the southwestern end of this block.
3. The geologic block adjacent to Fault 2 at the eastern end of the 3D seismic survey area is subsiding against the inverted triangular geologic block and dips to the northeast. In contrast, the block adjacent to the west side of Fault 1 is also subsiding against the inverted triangular geologic block and dips to the northwest. The latter geologic block forms a half-graben structure with Fault 1 as the main fault.
4. As a result of amplitude RMS attribute analysis on the 3D seismic data, we succeeded in extracting an old river channel from a geological unit underlying the base of the Holocene. The flow direction of this old river channel seems to northwest to northeast in the 3D seismic data area.
5. The depths of the old river channel are in the range of around 86 m from the sea surface. However, it was also detected at a depth of ca. 76 m at the southern end of the geological block between two faults (i.e., Faults 1 and 2). The latter portion is about 10 m shallower than the surrounding areas, implying pop-up of a faulted block after the periods of channel growth.
6. The estimated flow direction of the old river channel is northeastward, but the Holocene base and modern seafloor tend to incline northwestward, so it is difficult to imagine a river flowing northeastward at this location. This fact suggests that a tectonic event provoking northwestward subsidence in the geological block west of Fault 1 may have been underway since the period of the ancient river flow.

## **Author details**


Yasuto Itoh<sup>1\*</sup>, Akio Hara<sup>2</sup> and Taiki Sawada<sup>2</sup>

1 Osaka Metropolitan University, Osaka, Japan

2 JGI, Inc., Tokyo, Japan

\*Address all correspondence to: yasutokov@yahoo.co.jp

## **IntechOpen**

© 2023 The Author(s). Licensee IntechOpen. Distributed under the terms of the Creative Commons Attribution - NonCommercial 4.0 License (<https://creativecommons.org/licenses/by-nc/4.0/>), which permits use, distribution and reproduction for non-commercial purposes, provided the original is properly cited. 

## References

- [1] MEXT (Ministry of Education, Culture, Sports, Science and Technology, Japan), Graduate School of Science at Kyoto University. Comprehensive Research and Survey for the Beppu-Haneyama Fault System (Oita Plain – Eastern Part of Yufuin Fault), Heisei 26-28 Fiscal Year Report. Kyoto: Graduate School of Science at Kyoto University; 2017. Available from: [https://www.jishin.go.jp/database/project\\_report/beppu\\_haneyama/](https://www.jishin.go.jp/database/project_report/beppu_haneyama/)
- [2] Itoh Y, Inaba M. Fault-Controlled Processes of Basin Evolution: A Case on a Longstanding Tectonic Line. New York: Nova Science Publishers, Inc.; 2019. p. 81
- [3] Itoh Y, Kusumoto S, Takemura K. Evolutionary process of Beppu Bay in Central Kyushu, Japan: A quantitative study of the basin-forming process controlled by plate convergence modes. *Earth, Planets and Space*. 2014;**66**:74. Available from: <http://www.earth-planets-space.com/content/66/1/74>
- [4] Itoh Y, Takemura K, Kamata H. History of basin formation and tectonic evolution at the termination of a large transcurrent fault system: Deformation mode of Central Kyushu, Japan. *Tectonophysics*. 1998;**284**:135-150
- [5] Shimazaki K, Nakata T, Chida N, Miyatake T, Okamura M, Shiragami H, et al. A preliminary report on the drilling project of submarine active faults beneath Beppu Bay, Southwest Japan, for longterm earthquake prediction. *Active Fault Research*. 1986;**2**:83-88
- [6] Yoshioka T, Hoshizumi H, Miyazaki K. Geology of the Oita District with Geological Sheet Map at 1:50,000. Tsukuba: Geological Survey of Japan, AIST; 1997. p. 65
- [7] Ishizuka Y, Mizuno K, Matsuura H, Hoshizumi H. Geology of the Bungo-Kitsuki District with Geological Sheet Map at 1:50,000. Tsukuba: Geological Survey of Japan, AIST; 2005. p. 83
- [8] Itoh Y, Takemura K, Ishiyama T, Tanaka Y, Iwaki H. Basin formation at a contractional bend of a large transcurrent fault: Plio-Pleistocene subsidence of the Kobe and northern Osaka Basins, Japan. *Tectonophysics*. 2000;**321**:327-341
- [9] Itoh Y, Takemura K. Three-Dimensional Architecture and Paleoenvironments of Osaka Bay - An Integrated Seismic Study on the Evolutionary Processes of a Tectonic Basin. Singapore: Springer Nature Singapore Pte Ltd.; 2019. p. 119
- [10] Lisiecki LE, Raymo ME. A Pliocene-Pleistocene stack of 57 globally distributed benthic  $\delta^{18}\text{O}$  records. *Paleoceanography*. 2005;**20**:PA1003. DOI: 10.1029/2004PA001071
- [11] Noda A. Strike-slip basin - its configuration and sedimentary facies. In: Itoh Y, editor. *Mechanism of Sedimentary Basin Formation – Multidisciplinary Approach on Active Plate Margins*. Rijeka: IntechOpen; 2013. DOI: 10.5772/56593
- [12] Noda A, Toshimitsu S. Backward stacking of submarine channel-fan successions controlled by strike-slip faulting: The Izumi Group (Cretaceous), Southwest Japan. *Lithosphere*. 2009;**1**(1):41-59. DOI: 10.1130/L19.1
- [13] Yusa Y, Takemura K, Kitaoka K, Kamiyama K, Horie S, Nakagawa I, et al. Subsurface structure of Beppu Bay (Kyushu, Japan) by seismic reflection



and gravity survey. Zisin (Bulletin of Seismological Society of Japan). 1992;**45**:199-212

[14] Rao PH, Hansa GL, Savanur S, Mangal S, Ramegowda B, Shanker L, et al. Detection of thin sandstone reservoirs using multi attribute analysis and spectral decomposition on post stack 3D seismic data, north Sarbhan oil field, south Cambay basin, Gujarat, India. In: Proceedings of 5th Conference & Exposition on Petroleum Geophysics, Hyderabad-2004. Hyderabad, India: Society of Petroleum Geophysicists; 2004. pp. 752-759

[15] Azeem T, Wang Y, Khalid P, Liu X, Fang Y, Cheng L. An application of seismic attributes analysis for mapping of gas bearing sand zones in the Sawan gas field, Pakistan. *Acta Geodaetica et Geophysica*. 2016;**51**:723-744. DOI: 10.1007/s40328-015-0155-z

IntechOpen